
Article:
Zhu, Y., Yun, X. and Gardner, L. (2023) Behaviour, finite element modelling and design of high strength steel homogeneous and hybrid welded I-section beams. ce/papers, 6 (3-4). pp. 539-544. ISSN 2509-7075

https://doi.org/10.1002/cepa.2340

Behaviour, finite element modelling and design of high strength steel homogeneous and hybrid welded I-section beams

Yufei Zhu[1] | Xiang Yun[2] | Leroy Gardner[1]

1 Introduction

HSS I-sections are generally fabricated by welding together two flange plates and a web plate, enabling the use of different steel grades for the flanges and the web. For structural members that resist primarily bending moment, hybrid HSS welded I-sections, in which the flange plates are made of a higher strength steel than the web, are often more cost-effective than their homogenous HSS counterparts since the web of a cross-section only contributes a modest amount to the total bending resistance; hence, it can be more economical to use a less expensive lower strength steel in the web than in the flanges. While there is a strong body of research on homogeneous HSS welded I-section columns, a relatively limited number of studies have been performed on the flexural behaviour of HSS homogeneous and hybrid welded I-section beams [1-5].

The current design provisions given in EN 1993-1-12 [6] for HSS structures with steel grades up to S700 generally follow the design of NSS structures in EN 1993-1-1 [7], but with some restrictions. In the context of cross-section classification and design, the slenderness limits for HSS cross-sections are the same as those for NSS cross-sections, but plastic design is currently not permitted for HSS structures. The objectives of the present study are, therefore, to evaluate the accuracy of the current Eurocode slenderness limits for application to HSS homogeneous and hybrid welded I-sections and to assess the potential use of plastic design for HSS structures in light of a newly assembled pool of experimental and numerical results.

The present investigation features experimental, numerical and design-oriented studies into HSS beams. A total of six in-plane three-point bending tests on HSS homogeneous and hybrid welded I-sections are first described in Section 2. The beam specimens were bent about the major axis and a bespoke restraint rig was employed to prevent out-of-plane instability. Following the experimental study, finite element (FE) models were established and validated

against the test results obtained from the present study as well as those collected from the literature [2], as described in Section 3. The validated FE models were used to perform a series of parametric studies to generate supplementary numerical data on HSS homogeneous and hybrid welded I-section beams, covering a wide range of cross-section aspect ratios, cross-section slendernesses, loading configurations and steel grades. Based on the obtained test and FE results, the rotation capacity of HSS homogeneous and hybrid welded I-section beams was investigated and the suitability of the current Eurocode slenderness limits [6] was assessed.

2 Experimental programme

2.1 General

A total of six three-point major axis bending tests, with two on each of the three investigated welded I-section profiles (i.e. HSS-I-65×116×8×8, HSS-I-80×136×8×8 and HYB-I-80×136×8×8), were conducted. Three-point bending tests were chosen to investigate the bending resistance and rotation capacity of the studied cross-sections under a moment gradient; this is a common scenario in plastic designed frames. Each beam specimen was labelled by a unique identifier, e.g. HSS-I-65×116×8×8-3PB, where HSS-I (or HYB-I) denotes a homogeneous HSS welded I-section made of S690 steel for both its flanges and web (or a hybrid welded I-section with its flanges made of S690 steel and web made of S355 steel), 65×116×8×8 are the nominal dimensions of the welded I-section in millimetres (i.e. flange width B × outer section height H × flange thickness t_f × web thickness t_w) as illustrated in Figure 1, and 3PB represents three-point bending tests. For repeated tests, the letter "R" is added as a suffix to the specimen identifier. All three welded I-section sizes were fabricated from 8 mm-thick quenched and tempered S690 steel plates and hot-rolled S355 steel plates by means of gas metal arc welding with a nominal weld leg length (t_{weld}) of 5.6 mm (i.e. a weld throat thickness of 4 mm), as shown in Figure 1.

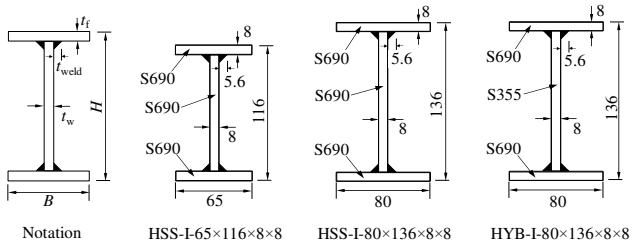

Figure 1 Notation and nominal dimensions of the three investigated welded I-sections (dimensions in mm).

2.2 Material testing

Prior to the bending tests, tensile coupon tests were conducted to obtain the key material properties and full-range stress-strain responses of the studied S690 and S355 steels. Details regarding the geometrical dimensions of the coupon specimens, the test arrangements and the measured full-range stress-strain curves were reported by the authors in [8-10], while the key average material properties for each steel grade are reported in Table 1, where E is the Young's modulus, f_y is the yield strength, f_u is the ultimate strength, ε_y is the yield strain, ε_{sh} is the strain hardening strain, ε_u is the strain corresponding to the ultimate strength, and ε_f is the strain at fracture (i.e. measured over a gauge length of 140 mm).

Table 1 Key average material properties for S355 and S690 steels from tensile coupon tests.

Steel grade	E	f_y	f_u	ε_y	ε_{sh}	ε_u	ε_f
	N/mm²	N/mm²	N/mm²	%	%	%	%
S355	198500	404.1	553.5	0.20	1.89	17.22	34.8
S690	212000	782.5	828.4	0.37	0.96	6.17	17.3

2.3 Three-point bending tests

The nominal length of all beam specimens L was 3200 mm, with an overhang of 100 mm at each end beyond the corresponding roller support, resulting in a span of L_{span} = 3000 mm for each tested specimen. The average measured geometrical dimensions for each beam specimen are reported in Table 2. The three investigated welded I-sections are all Class 1 cross-sections under pure bending according to the slenderness limits specified in prEN 1993-1-1: 2018 [11]. Each beam specimen was simply supported between a pair of steel rollers, which permitted the beam ends to undergo rotations about the axis of bending as well as longitudinal displacements, as shown in Figure 2. The tested beam specimens were loaded at mid-span using an Instron 250 kN testing machine under displacement control at a vertical displacement rate of 2.0 mm/min. Stiffeners and bearing plates were welded at the mid-span and the ends of the beam specimens to prevent web crippling under concentrated transverse loading. A bespoke lateral restraint system was designed and employed to prevent lateral and torsional deformations of the beam specimens and hence to prevent lateral-torsional buckling (LTB), as shown in Figure 2. The same lateral restraint system has also been successfully employed in previous HSS frame tests [8].

Table 2 Average measured geometrical dimensions and cross-sectional properties of beam specimens

Beam specimen	L	L_{span}	B	H	t_f	t_w
	mm	mm	mm	mm	mm	mm
HSS-I-65×116×8×8-3PB	3200	3000	64.42	116.31	8.40	8.45
HSS-I-65×116×8×8-3PB-R	3200	3000	62.22	116.50	8.40	8.42
HSS-I-80×136×8×8-3PB	3200	3000	79.59	136.67	8.41	8.43
HSS-I-80×136×8×8-3PB-R	3200	3000	79.42	136.75	8.44	8.44
HYB-I-80×136×8×8-3PB	3200	3000	79.71	136.72	8.40	8.08
HYB-I-80×136×8×8-3PB-R	3200	3000	79.61	136.65	8.37	8.18

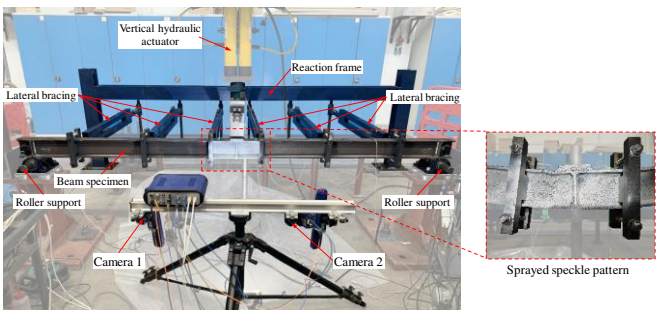

Figure 2 Configuration of beam specimens, experimental setup and DIC setup for major axis three-point bending tests.

Four strain gauges were affixed to the top and bottom flanges of the beam sections, at a distance of 50 mm from the stiffened mid-span section to monitor the strain development histories during testing. A string potentiometer was attached to the bottom flange of the beam at mid-span to record the vertical deformation of the beam during loading. Two inclinometers were mounted onto the webs of the extended overhangs to record the end rotations about the bending axis. The test outputs, including the applied vertical load and readings from the strain gauges, string potentiometer and inclinometers were recorded at 2-second intervals using the data acquisition equipment DATASCAN.

To gain further insight into the strain development at the mid-span region of the beam specimens where inelastic local buckling occurred, in addition to the traditional instrumentation described above, a two-camera digital image correlation (DIC) system was employed, as shown in Figure 2, where two cameras, with the focal lengths set to 35 mm, were utilised for the image acquisition. Prior to testing, the mid-span region of all beam specimens was painted white and then sprayed with a random black speckle pattern, as shown in Figure 2. Images were taken at 2-second intervals and processed using the DaVis version 8.4.0 imaging software [12].

Table 3 Key experimental results from three-point bending tests.

Beam specimen	M_u kNm	M_u/M_{pl} -	φ_{pl} rad	φ_u rad	R -
HSS-I-65×116×8×8-3PB	69.48	1.05	0.11	0.35	>2.14
HSS-I-65×116×8×8-3PB-R	67.50	1.05	0.11	0.35	>2.23
HSS-I-80×136×8×8-3PB	100.96	1.05	0.10	0.30	>1.93
HSS-I-80×136×8×8-3PB-R	100.91	1.05	0.11	0.28	>1.67
HYB-I-80×136×8×8-3PB	91.36	1.12	0.09	0.30	>2.50
HYB-I-80×136×8×8-3PB-R	90.78	1.11	0.08	0.32	>2.91

All the tested beam specimens failed by inelastic local buckling in the maximum moment region adjacent to the stiffened mid-span. The mid-span bending moment M was calculated from the applied vertical load, with allowance for the horizontal movement at the supports [13], and the mid-span rotation φ was determined as the sum of the end rotations recorded by the two inclinometers at the overhangs. The key test results are summarised in Table 3, where M_u is the ultimate bending moment at mid-span, φ_{pl} is the elastic component of the mid-span rotation when M_{pl} is first attained, determined by Eq. (1), φ_u is the mid-span rotation at M_u and R is the rotation capacity. The rotation capacity R is defined by Eq. (2), where φ_{rot} is the mid-span rotation when the moment at mid-span falls below M_{pl} on the descending branch. Note that the maximum recorded rotation φ_{max}, instead of φ_{rot}, was employed in Eq. (2) to calculate the rotation capacities of the presented three-point bending tests since these tests exceeded their peak moments, but were discontinued prior to the bending moment dropping below M_{pl}; the obtained rotation capacities may therefore be considered to be lower bounds. The rotation capacity for beams in four-point bending is defined using the method employed in many previous studies [13-15].

$$\varphi_{pl}=\frac{M_{pl}L_{span}}{2EI} \qquad (1)$$

$$R=\frac{\varphi_{rot}}{\varphi_{pl}}-1 \qquad (2)$$

The accuracy of the measurements obtained from the DIC system has been confirmed by comparing the displacement and strain histories obtained from the DIC system to those measured from the string potentiometers and strain gauges, respectively, at the corresponding location of each beam specimen. A more detailed description of the DIC validation has been reported by Yun et al. [8]. The longitudinal strain fields within the mid-span regions of a typical beam specimen – HSS-I-80×136×8×8-3PB, obtained from the DIC analyses at two representative load levels: (1) the load at which the mid-span bending moment reached the elastic bending moment M_{el}, and (2) the maximum applied load corresponding to M_u, are displayed in Figure 3, where the development of the inelastic local buckling can be observed. Note that the positive and negative strains in Figure 3 represent tensile strains and compressive strains, respectively.

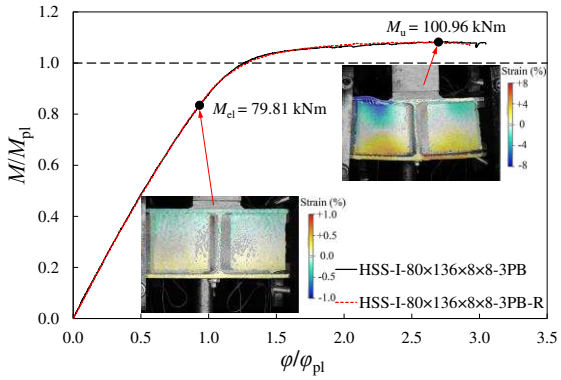

a) HSS-I-65×116×8×8-3PB and HSS-I-65×116×8×8-3PB-R

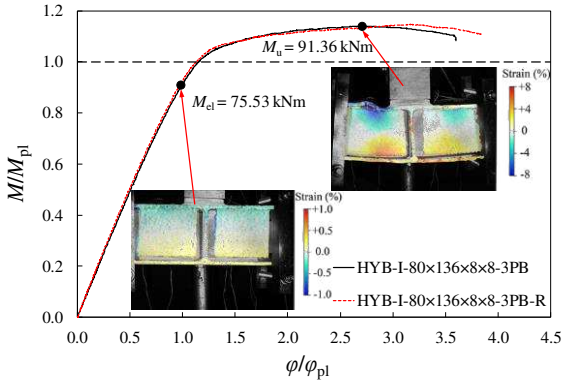

b) HYB-I-80×136×8×8-3PB and HYB-I-80×136×8×8-3PB-R

Figure 3 Normalised mid-span bending moment-mid-span rotation curves and longitudinal strain fields at different representative loads obtained from DIC for three-point bending specimens.

3 Numerical simulations

3.1 Basic modelling assumptions

In parallel with the experimental studies, comprehensive numerical simulations were performed to investigate the in-plane flexural behaviour of HSS homogeneous and hybrid welded I-section beams using the finite element (FE) analysis software ABAQUS [16]. The four-noded shell element S4R with reduced integration and finite membrane

strains was used for all simulations in the present study. A mesh size of (B+H)/40 which provided accurate results at reasonable computational cost, was selected to discretize the FE models. The measured or generated engineering stress-strain curves were transformed into true stress-logarithmic plastic strain curves prior to incorporation into ABAQUS. Residual stresses, determined from a residual stress pattern proposed in [10] for welded I-sections with varying steel grades, were introduced into the FE models as an initial stress condition.

Initial geometric imperfections were introduced into the developed FE models by modifying the nodal coordinates of the perfect geometry. Local geometric imperfections were assigned to the FE models in a sinusoidal shape with a half-wavelength $L_{b,cs}$, as shown in Figure 4. The local imperfection half-wavelength $L_{b,cs}$ was set equal to the elastic local buckling half-wavelength of the welded I-section in compression, which was determined using the finite strip software CUFSM [17], ensuring that an integer number of half-wavelengths were fitted within the member length. The modelling techniques have been described in [9] with the magnitudes of the local geometric imperfections taken equal to the tolerance-based values recommended in Annex C of EN 1993-1-5 [18] (see Figure 4). The use of tolerance-based imperfection amplitudes would be expected to yield slightly conservative resistance predictions in comparison to experimental results.

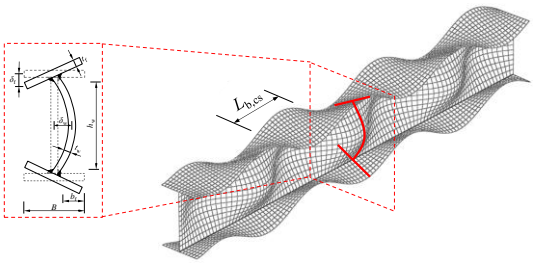

Figure 4 Definition of shape and amplitude of local geometric imperfections (not to scale) employed in FE models.

Suitable boundary and loading conditions were employed in the FE models to mimic the corresponding test setup, as described in Section 2.3 for the three-point bending tests and reported in [2] for the four-point bending tests. Stiffeners were also modelled at the loading and support sections where concentrated loads were applied in order to prevent localised web crippling failure, as employed in the tests. The out-of-plane displacement degree of freedom of the nodes located at the cross-sections where lateral restraints were provided was also constrained to prevent lateral-torsional buckling. The modified Riks method was employed for the geometrically and materially nonlinear analyses (GMNIA), enabling the post-ultimate response of the modelled specimens to be tracked.

3.2 Validation of FE models

The developed FE models were validated against the results from the three-point bending tests described in Section 2.3 and the four-point bending tests reported in [2] in terms of ultimate bending moments, full moment-deformation histories and failure modes. The ultimate bending moments derived from the FE models $M_{u.FE}$ are plotted against the results from the three-point and four-point bending tests $M_{u.test}$ in Figure 5, indicating good agreement, with the mean value of the ratio of $M_{u.test}/M_{u.FE}$ being 0.98 and the corresponding coefficient of variation being 0.02. It can thus be concluded that the established FE models are capable of replicating the flexural behaviour of the homogeneous and hybrid HSS welded I-section beams subjected to major axis bending.

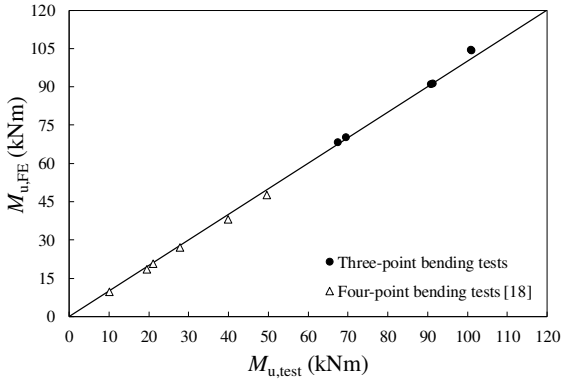

Figure 5 Comparison between ultimate bending moments obtained from FE models $M_{u.FE}$ and tests $M_{u.test}$.

3.3 Parametric studies

Upon the validation of the developed FE models, parametric studies were conducted with the aim of expanding the experimental data pool for homogeneous and hybrid welded I-section beams over a wide range of cross-section aspect ratios, cross-section slendernesses, steel grades and loading configurations. The ranges of variation of parameters considered in the parametric studies are listed in Table 4. The bilinear plus nonlinear hardening material model developed by Yun and Gardner [19] was utilised to represent the full-range stress-strain curves of the S355, S460 and S690 steels. The basic material properties (i.e. E, f_y and f_u) for the S355, S460 and S690 steels used in the parametric studies were taken as the nominal values given in prEN 1993-1-1: 2018 [11], as listed in Table 5, while the full-range stress-strain curves as well as the other key material properties such as ε_u and ε_{sh}, were derived using the predictive model set out in [19]. Lateral torsional buckling has been effectively prevented through use of suitable lateral restraints. The lateral restraints were applied at the top and bottom web-to-flange junctions of the sections in order to avoid any influence on the local buckling behaviour of the beam specimens. In total, 800 FE results on welded I-section beams were generated and are presented and analysed in the following section.

Table 4 Ranges of variation of parameters considered in parametric studies.

Material combination (Flange / Web)	B mm	H mm	t_f mm	t_w mm	t_{weld} mm	L_{span} mm
S690 / S690 S460 / S460 S355 / S355 S690 / S355 S690 / S355	100	100/150/ 200/300	3.4-17	0.6t_f	5.6	15H

Table 5 Summary of key material properties for S355, S460 and S690 steels employed in parametric studies.

Steel grade	E	f_y	f_u	f_u/f_y	ε_u	ε_{sh}
	N/mm²	N/mm²	N/mm²	-	-	-
S355	210000	355	490	1.38	0.17	0.017
S460	210000	460	540	1.17	0.09	0.030
S690	210000	690	770	1.12	0.06	0.030

4 Data analysis and design recommendations

4.1 General

In the following sections, the suitability of the current codified slenderness limits in EN 1993-1-12 (EC3) [6] for the classification of HSS outstand plate elements in compression and HSS internal plate elements in bending is assessed using the experimental results from the previous literature and the present study together with the generated FE results. Note that throughout this section, rotation capacities have been determined from the numerical simulations using a reduced bending moment $0.95M_{pl}$ instead of the plastic bending moment M_{pl} and denoted $R_{0.95}$ (instead of R); the purpose of this is to provide a more stable measure of rotation capacity and avoid anomalies in the results, since the moment-rotation (curvature) curves for stocky beams are typically characterised by a long plateau (particularly in four-point bending) when the cross-section bending moment is in the region of the full plastic bending moment M_{pl} before descending. It is the length of the plateau region that dictates the ability of a cross-section to redistribute moments (rather than the specific value of moment attained), and hence this approach is deemed to be appropriate. The same approach has been employed previously by [14,20,21].

4.2 HSS homogeneous welded I-section beams

To assess the applicability of the current EC3 Class 2 and Class 3 slenderness limits for S690 steel outstand elements in compression and internal (i.e. web) elements in bending, the test and numerical ultimate bending moments M_u for welded I-section beams made of S690, S460 and S355 steels are firstly normalised by the cross-section plastic bending resistances M_{pl} and the cross-section elastic bending resistance M_{el}, respectively. The normalised ultimate bending moments are then plotted against the flange slenderness ($b_f/t_f\varepsilon_f$) and web slenderness ($h_w/t_w\varepsilon_w$) ratios, then compared with the current EC3 Class 2 and Class 3 slenderness limits. It is shown that the S355, S460 and S690 data points generally follow the same trend, and the comparisons confirm the suitability of applying the current EC3 Class 2 and Class 3 slenderness limits to S690 steel welded I-sections subjected to major axis bending.

To assess the current EC3 Class 1 slenderness limits, the rotation capacities from both the experiments (R) and FE models ($R_{0.95}$) are plotted against the flange slenderness ($b_f/t_f\varepsilon_f$) and web slenderness ($h_w/t_w\varepsilon_w$) ratios, then compared with the current EC3 Class 1 slenderness limits (i.e. $b_f/t_f\varepsilon_f$ = 9 for outstand elements in compression and $h_w/t_w\varepsilon_w$ = 72 for internal elements in bending) and the rotation capacity requirement of R_{req} = 3 for Class 1 cross-sections. Note that the use of R (instead of $R_{0.95}$) was retained for the experiments since rotation capacities were typically reported in the literature using this measure. The comparisons show that the current EC3 Class 1 slenderness limits appear somewhat unconservative for both NSS and HSS welded I-sections. Lower slenderness limits of $b_f/t_f\varepsilon_f$ = 8 for outstand elements in compression and $h_w/t_w\varepsilon_w$ = 60 for internal plate elements in bending are thus proposed to provide improved predictions of when R_{req} = 3 can be achieved for both NSS and HSS welded I-sections. The slightly stricter proposed slenderness limits are considered to be essential for HSS due to the lack of historical precedent in applying plastic design to HSS structures. The rotation capacities of the newly classified Class 1 cross-sections are plotted against their flange and web slenderness ratios in Figure 6a and 6b, respectively, together with the proposed Class 1 slenderness limits for outstand flanges (in compression) and internal elements (in bending), which provide predictions of when R_{req} = 3 can be achieved. Note that the data points shaded in yellow indicate tests carried out in the present study that were terminated prior to reaching the full rotation capacity R, while the data points corresponding to the cross-sections where the web is Class 2 or above are shaded in grey, since both the flange and web must be Class 1 for plastic design to be applied.

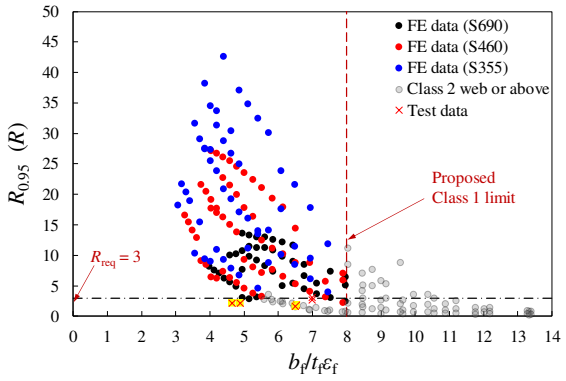

a) outstand plate elements in compression

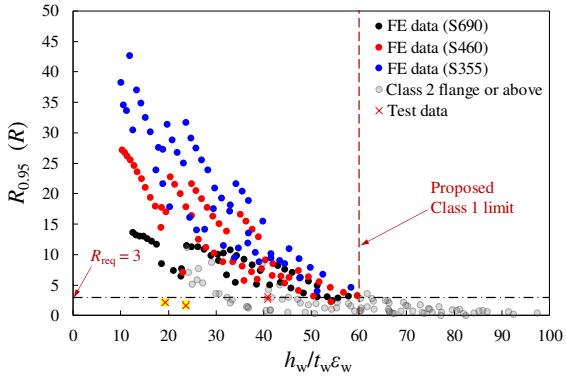

b) internal plate elements in bending

Figure 6 Examination of the proposed Class 1 slenderness limit for homogeneous welded I-section beams in three-point bending

4.3 HSS hybrid welded I-sections

The suitability of applying the current EC3 Class 2 and Class 3 slenderness limits and the newly proposed Class 1 slenderness limits to HSS hybrid welded I-sections is also evaluated using the same method presented in Section 4.2. The comparisons show that the current EC3 Class 2

and Class 3 slenderness limits for HSS welded I-sections are applicable to HSS hybrid welded I-sections subjected to major axis bending. The proposed more strict Class 1 slenderness limits for HSS homogeneous welded I-section beams are also suitable for the classification of HSS hybrid welded I-section beams in major axis bending.

5 Conclusions

Testing, finite element modelling and design aspects of high strength steel (HSS) beams have been described in this paper. An experimental programme, which included a total of six in-plane major axis three-point bending tests on both HSS homogeneous and hybrid welded I-sections, was carried out. The test setup, including the use of a bespoke restraint system to prevent lateral torsional buckling and the employment of DIC to monitor the strain histories of the most heavily loaded regions of the beam specimens, as well as the test results have been carefully presented and analysed. The test results obtained from the present study, as well as those collected from the literature, were subsequently employed in a parallel numerical modelling programme for the validation of FE models. An extensive parametric study was then carried out to generate additional structural performance data for the assessment of the influence of the material grade, cross-section aspect ratio and moment gradient on the flexural behaviour of HSS welded I-sections. The obtained test and FE results were also used to evaluate the applicability of the current EC3 cross-section classification limits [6] to both HSS homogeneous and hybrid welded I-sections subjected to major axis bending. It was confirmed that the current EC3 Class 2 and 3 slenderness limits are suitable to classify the outstand flanges (in compression) and internal webs (in bending) of both HSS homogeneous and hybrid welded I-sections. To satisfy the rotation capacity requirement of 3, stricter Class 1 slenderness limits for outstand flanges in compression (i.e. $b_f/t_f\varepsilon_f = 8$) and internal webs in bending ($h_w/t_w\varepsilon_w = 60$) were proposed; the use of the new limits is considered to be essential to allow the plastic design of HSS homogeneous and hybrid systems.

References

[1] Beg, D.; Hladnik, L. (1996) *Slenderness limit of class 3 I cross-sections made of high strength steel*. J Constr Steel Res, 38(3), 201-217.

[2] Sun, Y.; He, A.; Liang, Y.T. et al. (2019) *In-plane bending behaviour and capacities of S690 high strength steel welded I-section beams.* J Constr Steel Res,162,105741.

[3] Bartsch, H.; Eyben, F.; Pauli, G. et al. (2021) *Experimental and numerical investigations on the rotation capacity of high-strength steel beams*. J Struct Eng, 147(6), 04021067.

[4] Suzuki, T.; Ogawa, T.; Ikarashi, K. (1994) *A study on local buckling behavior of hybrid beams*. Thin-Wall Struct, 19(2-4), 337-351.

[5] Shokouhian, M.; Shi, Y. (2015) *Flexural strength of hybrid steel I-beams based on slenderness*. Eng Struct, 93, 114-28.

[6] EN 1993-1-12:2007. (2007) *Eurocode 3: Design of steel structures – Part 1-12: Additional rules for the extension of EN 1993 up to steel grades S700*. Brussels.

[7] EN 1993-1-1:2005. (2005) *Eurocode 3: Design of steel structures – Part 1-1: General rules and rules for buildings*. Brussels.

[8] Yun, X.; Zhu, Y.F.; Wang, Z.X. et al. (2022) *Benchmark tests on high strength steel I-section frames*. Eng Struct, 258, 114108.

[9] Zhu, Y.; Yun, X.; Gardner, L. (2023) *Behaviour and Design of High Strength Steel Homogeneous and Hybrid Welded I-Section Beams*. Eng Struct, 275, 115275.

[10] Yun, X.; Zhu, Y.F.; Meng, X. et al. (2023) *Welded steel I-section columns: Residual stresses, testing, simulation and design*. Eng Struct, 282, 115631.

[11] prEN 1993-1-1:2018. (2018) *Eurocode 3: Design of steel structures – Part 1-1: General rules and rules for buildings*. Brussels.

[12] LaVision (2017) *DaVis 8.4.* [software].

[13] Meng, X.; Gardner, L. (2020) *Cross-sectional behaviour of cold-formed high strength steel circular hollow sections*. Thin-Walled Struct, 156, 106822.

[14] Chan, T.M.; Gardner, L. (2008) *Bending strength of hot-rolled elliptical hollow sections*. J Constr Steel Res, 64, 971-986.

[15] Wang, J.; Afshan, S.; Gkantou, M. et al. (2016) *Flexural behaviour of hot-finished high strength steel square and rectangular hollow sections*. J Constr Steel Res, 121, 97-109.

[16] Dassault Systemes Simulia Corporation (2018) *Abaqus 2018* [software].

[17] Schafer, B.; Ádány, S. (2006) *Buckling analysis of cold-formed steel members using CUFSM: conventional and constrained finite strip methods*. Proceedings of the 18th International Specialty Conference on Cold-Formed Steel Structures. Orlando, pp. 39-54.

[18] EN 1993-1-5:2006. (2006) *Eurocode 3: Design of steel structures – Part 1-5: Plated structural elements*. Brussels; 2006.

[19] Yun, X.; Gardner, L. (2017) *Stress-strain curves for hot-rolled steels*. J Constr Steel Res, 133, 36-46.

[20] Lay, M.G.; Galambos, T.V. (1965) *Inelastic steel beams under uniform moment*. J Struct Div, 91(6), 67-93.

[21] Bartsch, H.; Eyben, F.; Schaffrath S. et al. (2021) *On the plastic design of high-strength steel beams*. Steel Constr, 14, 222-235.